PAPER

Check for updates

Frontier molecular orbital engineering in spiro-based molecules: achieving aggregation-induced delayed fluorescence for non-doped OLEDs†

Xue Li, [ID] ‡[ab] Changshen Shi,‡[c] Yuhang Mo,[a] Jiancheng Rao,[ab] Lei Zhao,*[b] Hongkun Tian,[b] Ning Sun[c] and Junqiao Ding [ID] *[a]

Frontier molecular orbital engineering has been demonstrated to achieve aggregation-induced delayed fluorescence (AIDF) for non-doped OLEDs. As a proof of concept, a new model compound, AT-spiro-DMACF, is reported on the basis of the TXADO-spiro-DMACF reference by changing the spiro-linked moiety from thioxanthene dioxide to anthracen-9(10H)-one. Such a minor alteration makes the lowest unoccupied molecular orbital (LUMO) shift from the inner fluorene to the outer anthracen-9(10H)-one, while retaining the almost same highest occupied molecular orbital (HOMO) distribution. In this case, the intermolecular charge transfer between the HOMO and LUMO becomes favorable, leading to aggregation-induced emission and thermally activated delayed fluorescence. As a result of this AIDF nature, AT-spiro-DMACF achieves a good non-doped device performance with a peak external quantum efficiency of 9.8% (31.1 cd A^{-1}, 33.7 lm W^{-1}) and Commission Internationale de l'Eclairage coordinates of (0.35, 0.54). The result clearly indicates that frontier molecular orbital engineering is an effective strategy for the development of AIDF emitters that are suitable for non-doped OLEDs.

[a] *School of Chemical Science and Technology, Yunnan University, Kunming 650091, P. R. China. E-mail: dingjunqiao@ynu.edu.cn*

[b] *State Key Laboratory of Polymer Physics and Chemistry, Changchun Institute of Applied Chemistry, Chinese Academy of Sciences, Changchun 130022, P. R. China. E-mail: zhaol@ciac.ac.cn*

[c] *School of Physics and Astronomy, Yunnan University, Kunming 650091, P. R. China*

† Electronic supplementary information (ESI) available: Experimental details including measurements and characterizations, quantum chemical calculations, device fabrication and measurement, synthesis; extra figures or tables of NMR, MALDI-TOF, TGA, DSC, CV, and PL spectra in different polarity solvents, UV-vis absorption spectra and transient decay fitting curve, and power efficiency for the non-doped device. Crystallographic information of AT-spiro-DMACF. CCDC 2114927. For ESI and crystallographic data in CIF or other electronic format see DOI: 10.1039/d1tc05225j

‡ These authors contributed equally to this article.

1 Introduction

Nowadays thermally activated delayed fluorescence (TADF) has become one of the most important mechanisms for organic light-emitting diodes (OLEDs).[1–4] As third-generation electroluminescence (EL) materials, pure organic TADF molecules are able to harvest both singlet and triplet excitons generated under electric excitation to achieve a theoretical 100% internal quantum efficiency without the use of noble metals.[5–8] So far, numerous high-performance TADF OLEDs have been successfully reported, whose colors can be well tuned throughout the whole visible region.[9–13] However, they are mostly based on a doped device configuration that is adopted to overcome unwanted concentration quenching effects.[14,15] In such a case, neither the selection of the appropriate host nor the delicate control of the dopant content is an easy task, making them susceptible to poor device reproducibility and stability.[16] Therefore, it is highly desirable to design novel TADF emitters for non-doped devices free of any host.[17–20]

In our previous work,[21] a spiro-blocking strategy was proposed towards deep-blue TADF emitters that are suitable for non-doped OLEDs (Fig. 1). As for the developed TXADO-spiro-DMACF, 9,9-dimethylacridine and fluorene are used as the donor (D) and acceptor (A), respectively, to constitute a linear D–A–D emitter (DMACF), and thioxanthene dioxide (TXADO) is chosen as the blocking unit. Its highest occupied molecular orbital (HOMO) mainly localizes on 9,9-dimethylacridine, and the lowest unoccupied molecular orbital (LUMO) distribution is localized on fluorene rather than TXADO. That is, the spiro-linked TXADO does not contribute to the intramolecular charge transfer (CT) nature of the whole molecule but acts as a blocking unit to prevent intermolecular interactions. Benefitting from this spiro-blocking, the non-doped device of TXADO-spiro-DMACF gives deep-blue EL with a promising external quantum efficiency (EQE) of 5.3% (5.3 cd A^{-1}, 5.9 lm W^{-1}) as well as Commission Internationale de l'Eclairage (CIE) coordinates of (0.16, 0.09).

This journal is © The Royal Society of Chemistry 2022

J. Mater. Chem. C, 2022, **10**, 4845–4850 | **4845**

Fig. 1 The two design systems in spiro-based TADF molecules for non-doped OLEDs.

Based on the same spiro geometry (Fig. 1), herein we newly develop another model compound, AT-spiro-DMACF, when TXADO is replaced by anthracen-9(10H)-one (AT). After such a minor alternation, the LUMO distribution is found to move from the inner fluorene to the peripheral AT, while the HOMO still resides on the acridine moieties. Given the large space separation between the HOMO and the LUMO, intermolecular rather than intramolecular CT is anticipated to happen and play a key role in the photoluminescence (PL) of AT-spiro-DMACF. As a result, this compound shows interesting aggregation induced delayed fluorescence (AIDF), which is beneficial for the fabrication of non-doped OLEDs. With AT-spiro-DMACF as the host-free emitting layer, a good non-doped device performance is obtained, revealing a peak EQE of 9.8% (31.1 cd A^{-1}, 33.7 lm W^{-1}) and CIE coordinates of (0.35, 0.54). The result clearly indicates that frontier molecular orbital engineering is an effective method to realize AIDF for non-doped OLEDs.

2 Results and discussion

2.1 Synthesis and characterization

The synthetic route to AT-spiro-DMACF is presented in Scheme S1 (ESI†). Starting from 4,4′-dibromo-2-iodo-1,1′-biphenyl and anthracene-9,10-dione, the key intermediate 2′,7′-dibromo-10H-spiro[anthracene-9,9′-fluoren]-10-one (2) was first prepared via a Kumada reaction and cyclization in sequence.[22] Then palladium-catalyzed Buchwald–Hartwig coupling between 2 and 9,9-dimethylacridine was performed to produce the final

compound AT-spiro-DMACF in a yield of 85%. The molecular structure of AT-spiro-DMACF was fully confirmed via ^{1}H and ^{13}C NMR, MALDI-TOF mass spectrometry and elemental analysis (Fig. S1 and S2, ESI†).

Similar to TXADO-spiro-DMACF, AT-spiro-DMACF was thermally stable with a decomposition temperature (T_d; corresponding to a 5% weight loss) as high as 454 °C and no obvious glass transition in the range of 35–300 °C (Fig. S3, ESI†). Also, cyclic voltammetry (CV) was carried out in anhydrous dichloromethane. Only oxidation processes could be detected for AT-spiro-DMACF during the anodic scanning (Fig. S4, ESI†). Together with the optical bandgap estimated from the PL onset, its HOMO and LUMO energy levels are determined to be −5.33 and −2.48 eV, respectively (Table 1). In comparison with TXADO-spiro-DMACF, the LUMO of AT-spiro-DMACF is distinctly reduced by about 0.25 eV due to the stronger electron-withdrawing capability of AT over fluorene.

In addition, a single crystal of AT-spiro-DMACF was obtained via slow evaporation from a mixed solvent of dichloromethane and n-hexane. With respect to TXADO-spiro-DMACF, as depicted in Fig. 2, a similar crystal structure and packing is observed for AT-spiro-DMACF. Owing to their different LUMO distributions (Fig. 1), nevertheless, TXADO-spiro-DMACF and AT-spiro-DMACF show quite different CT routes between the HOMO and the LUMO, which is believed to be responsible for the PL. In TXADO-spiro-DMACF, for example, the LUMO is located not on the spiro-linked TXADO but on the inner fluorene. The spiro-blocking effect from TXADO may hamper the intermolecular CT from acridine in one molecule to fluorene in the adjacent two molecules (the mentioned moieties are marked with blue and red solid or dotted lines). So the intramolecular CT from acridine to fluorene in the same molecule does contribute to the PL of TXADO-spiro-DMACF, which is consistent with our previous work.[21] By contrast, the LUMO is distributed on the spiro-linked AT rather than the inner fluorene for AT-spiro-DMACF. Considering the large space separation between the HOMO and the LUMO, the possibility of intramolecular CT from acridine to AT in the same molecule may be neglected reasonably. This is further confirmed by the much smaller oscillator strength of AT-spiro-DMACF (f = 0.0016) relative to TXADO-spiro-DMACF (f = 0.0214, in Table S2, ESI†). However, under the driving force of the molecular packing, acridine in one molecule could come close to AT in another neighboring molecule. Therefore, the intermolecular CT between them is within our expectations, which will be discussed below.

Table 1 Comparison of the photophysical, electrochemical and thermal properties between TXADO-spiro-DMACF and AT-spiro-DMACF

	$\lambda_{abs}{}^{b}$ [nm]	$\lambda_{PL}{}^{c}$ [nm]	$\tau_p/\tau_d{}^{c}$ [ns/μs]	$\Phi_{PL}{}^{c}$	S$_1$/T$_1$/$\Delta E_{ST}{}^{d}$ [eV]	$E_g{}^{e}$ [eV]	HOMO/LUMO^{f} [eV]	$T_d{}^{g}$ [°C]
TXADO-spiro-DMACF^{a}	364	445	3.8/106	0.42	3.14/2.86/0.28	3.10	−5.33/−2.23	464
AT-spiro-DMACF	361	505	145/3.1	0.23	2.85/2.64/0.21	2.85	−5.33/−2.48	454

^{a} Data from ref. 21. ^{b} Measured in toluene solution (10^{-5} M). ^{c} Measured as a neat film. ^{d} S$_1$ and T$_1$ are determined from the onset of the fluorescence and phosphorescence spectra as a neat film, respectively; ΔE_{ST} is the energy difference between S$_1$ and T$_1$. ^{e} Optical bandgap estimated from the PL onset. ^{f} HOMO = −e[$E_{onset,ox}$ + 4.8] V, LUMO = HOMO + E_g, where $E_{onset,ox}$ is the onset value of the first oxidation. ^{g} Decomposition temperature corresponding to a 5% weight loss.

4846 | J. Mater. Chem. C, 2022, **10**, 4845–4850

This journal is © The Royal Society of Chemistry 2022
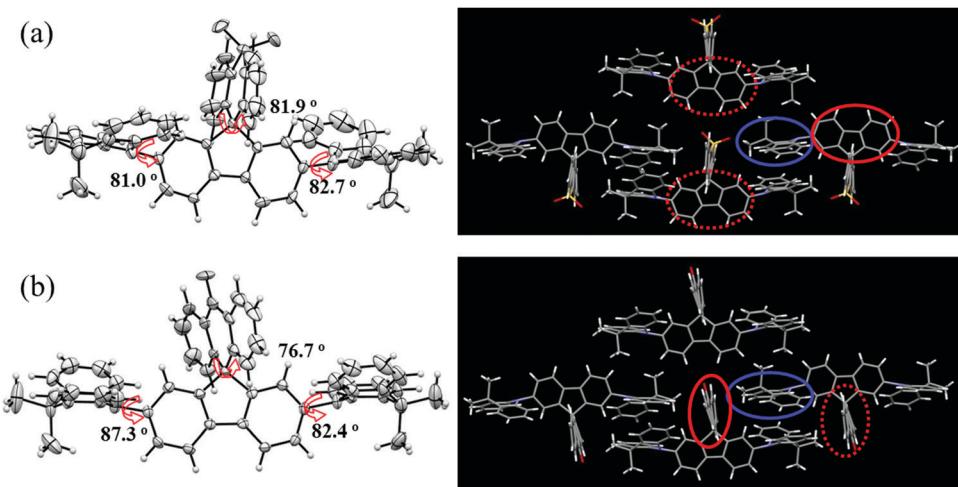
Fig. 2 Crystal structure and packing in TXADO-spiro-DMACF (a) and AT-spiro-DMACF (b). To indicate the possible CT route between the HOMO and the LUMO, the partial moieties are circled with blue and red solid lines (favorable) or dotted lines (unfavorable), respectively.

2.2 Photophysical properties

As presented in Fig. 3a, AT-spiro-DMACF exhibits two distinct absorption bands in toluene solution. The intense absorption bands below 330 nm can be assigned to the localized $\pi-\pi^*$ transitions, and the moderate absorption in the range of 330–400 nm is almost the same as that of TXADO-spiro-DMACF (Fig. S5a, ESI†).[21] Combined with their frontier molecular orbital distributions (Fig. S5b, ESI†), reasonably, this band originates from acridine-to-fluorene CT, corresponding to the HOMO → LUMO+1 transition. Noticeably, in going from solution to the solid state, an additional weak but discernible absorption tail also occurs, which is a good indicator of the above-mentioned intermolecular CT between the HOMO and the LUMO.

Furthermore, AT-spiro-DMACF displays a broad and structure-less fluorescence peak at 505 nm in the solid state. Moreover, its phosphorescence was also measured at 77 K and is plotted in Fig. 3a. According to their onset values, the singlet energy (S_1) and triplet energy (T_1) are taken to be 2.85 and 2.64 eV, respectively. The corresponding energy difference between S_1 and T_1 is as low as 0.21 eV, ensuring the efficient T_1-to-S_1 up-conversion and thus delayed fluorescence.[1,23] To demonstrate the TADF nature, the transient PL spectrum is recorded for the AT-spiro-DMACF neat film, and shows an obvious delayed fluorescence with a short lifetime of 3.1 μs (Fig. 3b and Fig. S6, ESI†). In addition, the delayed component below 15 μs initially increases from 50 to 200 K because of the thermally-promoted TADF, and then decreases from 200 to 300 K because of the weakened phosphorescence (Fig. S7, ESI†).[24,25] Different from the neat film, no TADF is detected for AT-spiro-DMACF in toluene (Fig. S8, ESI†). In good agreement with the above-mentioned frontier molecular orbital distribution and crystal packing, this observation clearly indicates the contribution from the intermolecular CT. This is further verified by the concentration-dependent PL decay of doped AT-spiro-DMACF films in polystyrene (PS). Meanwhile, the film PL quantum yield of AT-spiro-DMACF is determined to be 0.23 (Table 1). The moderate value is understandable when considering that intermolecular CT is not an efficient process although the crystal packing is proved to be favorable for the molecular approach.

Fig. 4 compares the PL spectra for TXADO-spiro-DMACF and AT-spiro-DMACF in a THF/water mixed solvent. As one can see,
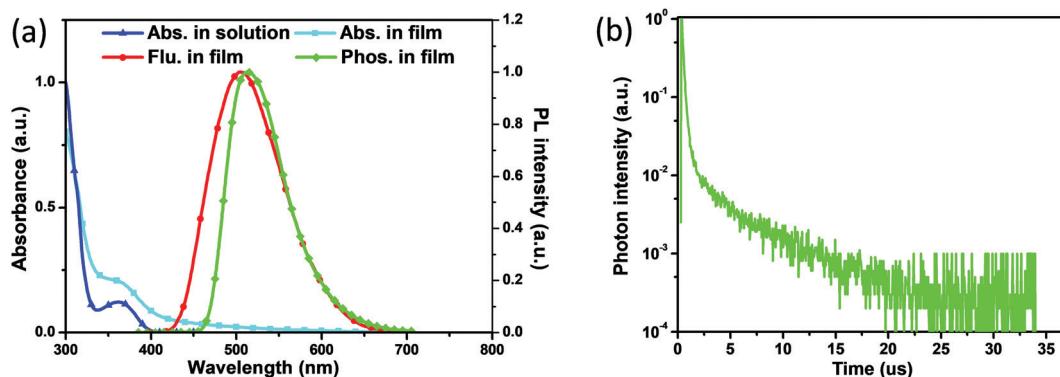

Fig. 3 Photophysical properties of AT-spiro-DMACF: (a) comparison of UV-Vis absorption in toluene solution and neat film, together with the film fluorescence spectrum at 298 K and phosphorescence spectrum at 77 K; and (b) transient PL spectrum in the neat film.

This journal is © The Royal Society of Chemistry 2022

J. Mater. Chem. C, 2022, 10, 4845–4850 | 4847
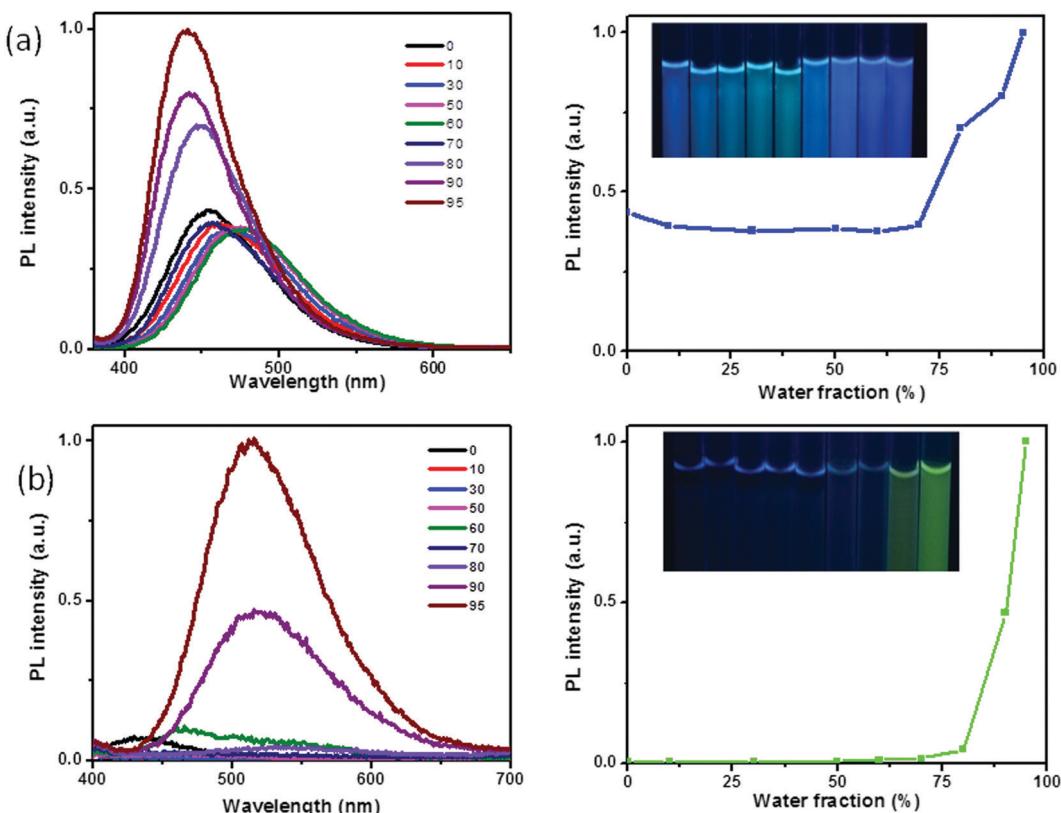
Fig. 4 Water-fraction dependence of PL spectra in a THF/water mixed solvent for TXADO-spiro-DMACF (a) and AT-spiro-DMACF (b). Inset: images of how the PL varies with different water fractions under 350 nm excitation.
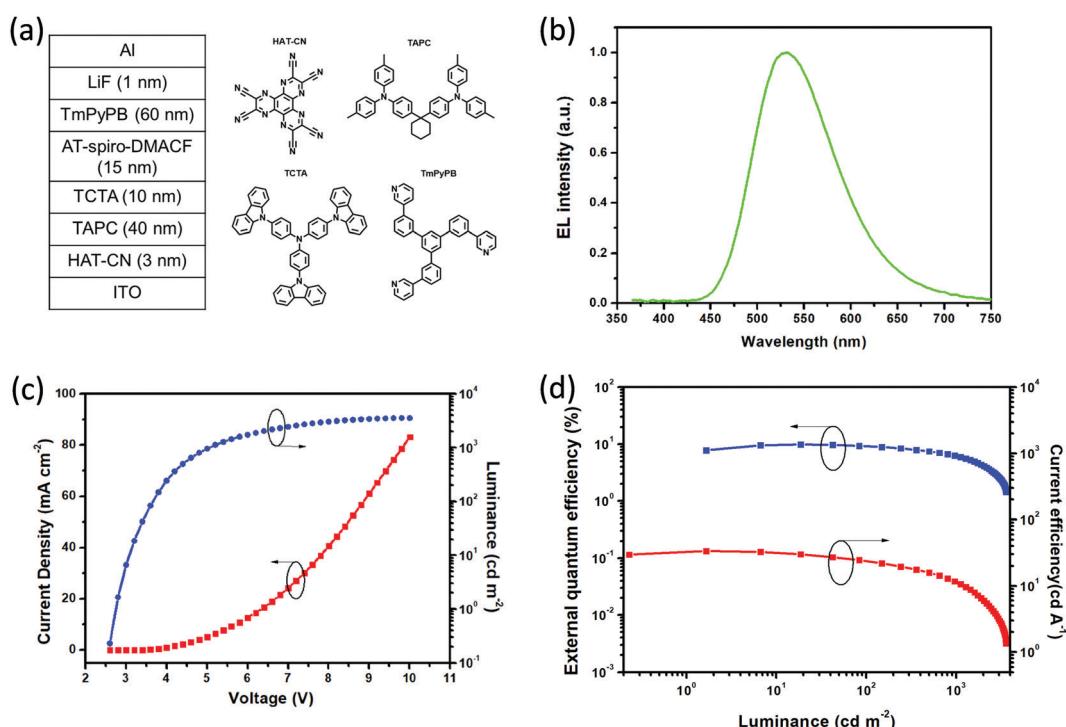

Fig. 5 Non-doped device performance for AT-spiro-DMACF: (a) device configuration and molecular structures of used materials; (b) EL spectrum at 5 V; (c) current density–voltage–luminance characteristics; and (d) EQE and current efficiency as a function of luminance.

TXADO-spiro-DMACF displays typical aggregation-enhanced emission (AEE) with the increasing water fraction (f_w). By contrast, AT-spiro-DMACF is nearly non-emissive in pure THF solution ($f_w = 0$). When f_w goes up to 0.95, the PL intensity is found to be dramatically increased, indicative of the aggregation-induced emission (AIE)[26–28] nature of AT-spiro-DMACF. The difference between TXADO-spiro-DMACF and AT-spiro-DMACF could be attributed to their different LUMO distributions. As discussed above, unlike TXADO-spiro-DMACF with mainly intramolecular CT, intermolecular CT between the HOMO and the LUMO turns out to be favorable in AT-spiro-DMACF. This is tentatively believed to result in the observed AIE behavior. Moreover, the CT character of AT-spiro-DMACF is verified by the positive solvatochromic effect and the linear correlation of the solvent orientation polarization with the Stokes shift (Fig. S9, ESI†).[29,30]

2.3 EL properties

In terms of the obtained AIDF (AIE and TADF) for AT-spiro-DMACF, the non-doped device was assembled on the basis of the configuration ITO/HATCN (3 nm)/TAPC (40 nm)/TCTA (10 nm)/EML (15 nm)/TmPyPB (60 nm)/LiQ (1 nm)/Al (Fig. 5a). Here, dipyrazino[2,3-*f*:2′,3′-*h*]quinoxaline-2,3,6,7,10,11-hexacarbonitrile (HATCN) and LiF are employed as the hole- and electron-injection layers, respectively; 4,4′-(cyclohexane-1,1-diyl)bis(*N*,*N*-di-*p*-tolylaniline (TAPC) and 1,3,5-tri[(3-pyridyl)-phen-3-yl]benzene (TmPyPB) are used as the hole- and electron-transporting layers, respectively; and 4,4′,4″-tris(carbazol-9-yl)triphenylamine (TCTA) is selected as the exciton-blocking layer. Moreover, the emitting layer (EML) is composed of AT-spiro-DMACF without any host.

Fig. 5b–d plot the EL spectrum, current density–voltage–luminance characteristics, EQE and current efficiency as a function of luminescence for the non-doped device of AT-spiro-DMACF. As can be clearly seen in Fig. 5b, AT-spiro-DMACF shows bright green EL with an emission maximum of about 532 nm and CIE coordinates of (0.35, 0.54). Compared with the PL counterpart (λ_{em} = 505 nm), the red-shift could be ascribed to the enhanced intermolecular interactions during the EL process, similar to exciplex-based OLEDs.[31] Moreover, due to the AIDF feature, the non-doped device of AT-spiro-DMACF possesses a low turn-on voltage of 2.8 V at 1 cd m^{-2} as well as a maximum luminance of 3565 cd m^{-2} (Fig. 5c). Correspondingly, a maximum current efficiency of 31.1 cd A^{-1}, a maximum power efficiency of 33.7 lm W^{-1} and a peak EQE of 9.8% are obtained, which are comparable to previously-reported TADF emitters that are suitable for non-doped OLEDs.[32,33] The EQE further decays to 6.3% at a high luminance of 1000 cd m^{-2}, indicating the efficiency roll-off caused by triplet–triplet annihilation (TTA) and/or triplet–polaron annihilation (TPA). In spite of this, AT-spiro-DMACF is distinctly superior to those of doped devices (Fig. S11 and Table S4, ESI†), highlighting the AIDF potential for non-doped OLEDs.

3 Conclusions

Starting from TXADO-spiro-DMACF with a spiro-blocking effect, in summary, the new model compound AT-spiro-DMACF has been designed and synthesized to realize interesting AIDF for non-doped OLEDs. After replacement of the spiro-linked TXADO moiety with AT, the LUMO distribution is found to shift from the inner fluorene to the outer AT, while the HOMO distribution remains on the acridine moieties. As a result of the large space separation between the HOMO and the LUMO, favorable intermolecular CT mainly contributes to the PL process of AT-spiro-DMACF, thus leading to AIE behavior. Meanwhile, this compound also shows obvious TADF with a delayed fluorescence lifetime of 3.1 μs. Benefitting from this AIDF nature, a moderate EQE of 9.8% is achieved for the non-doped device of AT-spiro-DMACF. This work, we believe, first correlates AIDF with frontier molecular orbital engineering and intermolecular CT, and will shed light on the development of AIDF emitters that are suitable for non-doped OLEDs.

Conflicts of interest

The authors declare no competing financial interest.

Acknowledgements

References

1 H. Uoyama, K. Goushi, K. Shizu, H. Nomura and C. Adachi, *Nature*, 2012, **492**, 234–238.

2 C. Adachi, *Jpn. J. Appl. Phys.*, 2014, **53**, 060101.

3 Y. C. Liu, C. S. Li, Z. J. Ren, S. K. Yan and M. R. Bryce, *Nat. Rev. Mater.*, 2018, **3**, 18020.

4 X. Yin, Y. He, X. Wang, Z. Wu, E. B. Pang, J. Xu and J. A. Wang, *Front. Chem.*, 2020, **8**, 725.

5 H. Kaji, H. Suzuki, T. Fukushima, K. Shizu, K. Suzuki, S. Kubo, T. Komino, H. Oiwa, F. Suzuki, A. Wakamiya, Y. Murata and C. Adachi, *Nat. Commun.*, 2015, **6**, 8476.

6 J.-X. Chen, W.-W. Tao, W.-C. Chen, Y.-F. Xiao, K. Wang, C. Cao, J. Yu, S. Li, F.-X. Geng, C. Adachi, C.-S. Lee and X.-H. Zhang, *Angew. Chem., Int. Ed.*, 2019, **58**, 14660–14665.

7 S. Hirata, Y. Sakai, K. Masui, H. Tanaka, S. Y. Lee, H. Nomura, N. Nakamura, M. Yasumatsu, H. Nakanotani, Q. Zhang, K. Shizu, H. Miyazaki and C. Adachi, *Nat. Mater.*, 2015, **14**, 330–336.

8 Q. S. Zhang, B. Li, S. P. Huang, H. Nomura, H. Tanaka and C. Adachi, *Nat. Photonics*, 2014, **8**, 326–332.

9 S. Kothavale, W. J. Chung and J. Y. Lee, *J. Mater. Chem. C*, 2020, **8**, 7059–7066.

10 T. A. Lin, T. Chatterjee, W. L. Tsai, W. K. Lee, M. J. Wu, M. Jiao, K. C. Pan, C. L. Yi, C. L. Chung, K. T. Wong and C. C. Wu, *Adv. Mater.*, 2016, **28**, 6976–6983.

11 J. C. Rao, L. Q. Yang, X. F. Li, L. Zhao, S. M. Wang, J. Q. Ding and L. X. Wang, *Angew. Chem., Int. Ed.*, 2020, **59**, 17903–17909.

This journal is © The Royal Society of Chemistry 2022

J. Mater. Chem. C, 2022, **10**, 4845–4850 | 4849

12 T. L. Wu, M. J. Huang, C. C. Lin, P. Y. Huang, T. Y. Chou, R. W. Chen-Cheng, H. W. Lin, R. S. Liu and C. H. Cheng, *Nat. Photonics*, 2018, **12**, 235–240.

13 Y. L. Zhang, Q. Ran, Q. Wang, Y. Liu, C. Hanisch, S. Reineke, J. Fan and L. S. Liao, *Adv. Mater.*, 2019, **31**, 1902368.

14 H. Q. Wang, B. J. Zhao, P. Ma, Z. Li, X. Y. Wang, C. X. Zhao, X. T. Fan, L. L. Tao, C. B. Duan, J. Zhang, C. M. Han, G. Y. Chen and H. Xu, *J. Mater. Chem. C*, 2019, **7**, 7525–7530.

15 W. L. Tsai, M. H. Huang, W. K. Lee, Y. J. Hsu, K. C. Pan, Y. H. Huang, H. C. Ting, M. Sarma, Y. Y. Ho, H. C. Hu, C. C. Chen, M. T. Lee, K. T. Wong and C. C. Wu, *Chem. Commun.*, 2015, **51**, 13662–13665.

16 Y. X. Wang, J. H. Yun, L. Wang and J. Y. Lee, *Adv. Funct. Mater.*, 2020, **31**, 2008332.

17 J. Guo, X.-L. Li, H. Nie, W. Luo, S. Gan, S. Hu, R. Hu, A. Qin, Z. Zhao, S.-J. Su and B.-Z. Tang, *Adv. Funct. Mater.*, 2017, **27**, 1606458.

18 Y. Z. Shi, K. Wang, X. Li, G. L. Dai, W. Liu, K. Ke, M. Zhang, S. L. Tao, C. J. Zheng, X. M. Ou and X. H. Zhang, *Angew. Chem., Int. Ed.*, 2018, **57**, 9480–9484.

19 J. Huang, H. Nie, J. Zeng, Z. Zhuang, S. Gan, Y. Cai, J. Guo, S.-J. Su, Z. Zhao and B.-Z. Tang, *Angew. Chem., Int. Ed.*, 2017, **56**, 12971–12976.

20 M. Godumala, S. Choi, M. J. Cho and D. H. Choi, *J. Mater. Chem. C*, 2019, **7**, 2172–2198.

21 J. C. Rao, C. Y. Zhao, Y. P. Wang, K. Y. Bai, S. M. Wang, J. Q. Ding and L. X. Wang, *ACS Omega*, 2019, **4**, 1861–1867.

22 K. Y. Bai, S. M. Wang, L. Zhao, J. Q. Ding and L. X. Wang, *Polym. Chem.*, 2017, **8**, 2182–2188.

23 Z. Y. Yang, Z. Mao, Z. L. Xie, Y. Zhang, S. W. Liu, J. Zhao, J. R. Xu, Z. G. Chi and M. P. Aldred, *Chem. Soc. Rev.*, 2017, **46**, 915–1016.

24 J. Li, T. Nakagawa, Q. S. Zhang, H. Nomura, H. Miyazaki and C. Adachi, *Adv. Mater.*, 2013, **25**, 3319–3323.

25 X. Li, J. C. Rao, L. Q. Yang, L. Zhao, S. M. Wang, H. K. Tian, J. Q. Ding and L. X. Wang, *Macromolecules*, 2021, **54**, 5260–5266.

26 X. D. Wang, S. M. Wang, J. H. Lv, S. Y. Shao, L. X. Wang, X. B. Jing and F. S. Wang, *Chem. Sci.*, 2019, **10**, 2915–2923.

27 X. D. Wang, J. Hu, J. H. Lv, Q. Q. Yang, H. K. Tian, S. Y. Shao, L. X. Wang, X. B. Jing and F. S. Wang, *Angew. Chem., Int. Ed.*, 2021, **60**, 16585–16593.

28 J. Guo, X.-L. Li, H. Nie, W. Luo, S. Gan, S. Hu, R. Hu, A. Qin, Z. Zhao, S.-J. Su and B. Z. Tang, *Adv. Funct. Mater.*, 2017, **27**, 1606458.

29 N. Mataga, Y. Kaifu and M. Koizumi, *Bull. Chem. Soc. Jpn.*, 1956, **29**, 465–470.

30 E. Lippert, *Ber. Bunsen-Ges.*, 1957, **61**, 962.

31 L. Gan, Z. D. Xu, Z. H. Wang, B. B. Li, W. Li, X. Y. Cai, K. K. Liu, Q. M. Liang and S.-J. Su, *Adv. Funct. Mater.*, 2019, **29**, 1808088.

32 X. Zhou, Y. P. Xiang, F. Ni, Y. Zou, Z. X. Chen, X. J. Yin, G. H. Xie, S. L. Gong and C. L. Yang, *Dyes Pigm.*, 2020, **176**, 108179.

33 F. L. Ma, Y. Cheng, Y. Zheng, H. F. Ji, K. Hasrat and Z. J. Qi, *J. Mater. Chem. C*, 2019, **7**, 9413–9422.

4850 | *J. Mater. Chem. C*, 2022, **10**, 4845–4850

This journal is © The Royal Society of Chemistry 2022